

Discovery of Highly Potent and Selective IRAK1 Degraders to Probe Scaffolding Functions of IRAK1 in ABC DLBCL

Liqiang Fu,[△] Jing Zhang,[△] Bin Shen, Linglong Kong, Yingtao Liu, Wangyang Tu, Wenqian Wang, Xin Cai, Xiaotao Wang, Na Cheng, Mingxuan Xia, Tianyuan Zhou, Qian Liu, Yanping Xu, Jennifer Yang, Paul Gavine, Ulrike Philippar, Ricardo Attar, James P. Edwards, Jennifer D. Venable,* and Xuedong Dai*



Cite This: <https://doi.org/10.1021/acs.jmedchem.1c00103>



Read Online

ACCESS |



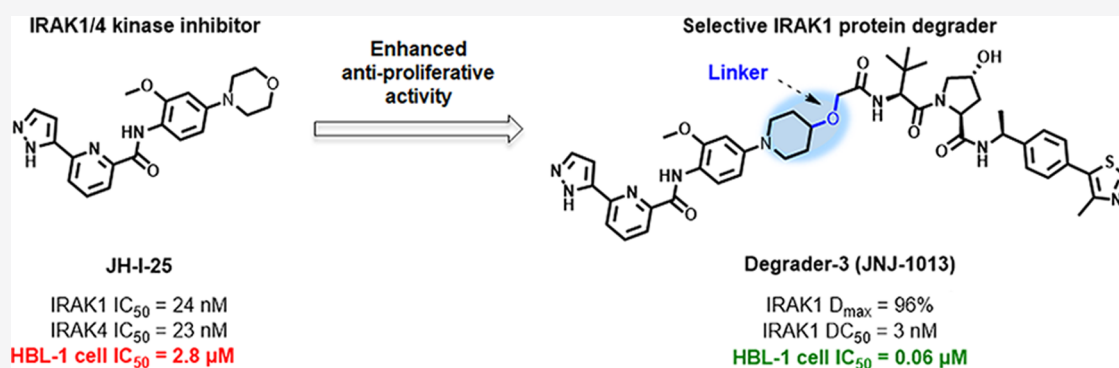
Metrics & More



Article Recommendations



Supporting Information



ABSTRACT: MyD88 gene mutation has been identified as one of the most prevalent driver mutations in the activated B-cell-like diffuse large B-cell lymphoma (ABC DLBCL). The published literature suggests that interleukin-1 receptor-associated kinase 1 (IRAK1) is an essential gene for ABC DLBCL harboring MyD88 mutation. Importantly, the scaffolding function of IRAK1, rather than its kinase activity, is required for tumor cell survival. Herein, we present our design, synthesis, and biological evaluation of a novel series of potent and selective IRAK1 degraders. One of the most potent compounds, **Degradar-3 (JNJ-1013)**, effectively degraded cellular IRAK1 protein with a DC₅₀ of 3 nM in HBL-1 cells. Furthermore, **JNJ-1013** potently inhibited IRAK1 downstream signaling pathways and demonstrated strong anti-proliferative effects in ABC DLBCL cells with MyD88 mutation. This work suggests that IRAK1 degraders have the potential for treating cancers that are dependent on the IRAK1 scaffolding function.

INTRODUCTION

Interleukin-1 receptor-activated kinases (IRAK1, IRAK2, IRAK3, and IRAK4) are serine/threonine kinases that mediate innate immune and inflammatory responses. IRAKs play important roles in transducing inflammatory signals downstream of the toll-like receptors (TLRs) and interleukin-1 receptors (IL-1Rs).¹ When activated, TLRs or IL-1Rs dimerize and recruit the myeloid differentiation primary response 88 (MyD88) adaptor protein through their intracellular domains. MyD88 further recruits IRAK4 and IRAK1/2 to form a multiprotein complex, namely, the Myddosome. IRAK4 phosphorylates IRAK1 to first prime its activity, leading to further activation, hyperphosphorylation, and dissociation from the Myddosome and subsequent interaction with the E3 ubiquitin ligase, TNF receptor-associated factor 6 (TRAF6). The activated TRAF6 complex in turn drives downstream events, including the IκB kinase (IKK)-nuclear factor-κB (NF-κB) and mitogen-activated protein kinase (MAPK) signaling pathways that ultimately result in the upregulation of proinflammatory cytokines.²

Diffuse large B-cell lymphoma (DLBCL) is the most common aggressive non-Hodgkin lymphoma (NHL), accounting for about 30–35% of NHL cases around the world. DLBCL can be divided into germinal center B-cell-like (GCB) and activated B-cell-like (ABC) subtypes.³ ABC DLBCL is associated with poor prognosis compared to the GCB subtype. MyD88 gain-of-function mutation frequently appears in ABC DLBCL, resulting in constitutive activation of the IRAK4- and IRAK1-mediated signaling.⁴ However, in our previous efforts to inhibit the MyD88 pathway, neither a selective IRAK4 kinase inhibitor nor a new series of potent and selective IRAK4 degraders that dismantle the IRAK4 scaffolding function demonstrated noticeable anti-proliferation effects. These

Received: January 20, 2021

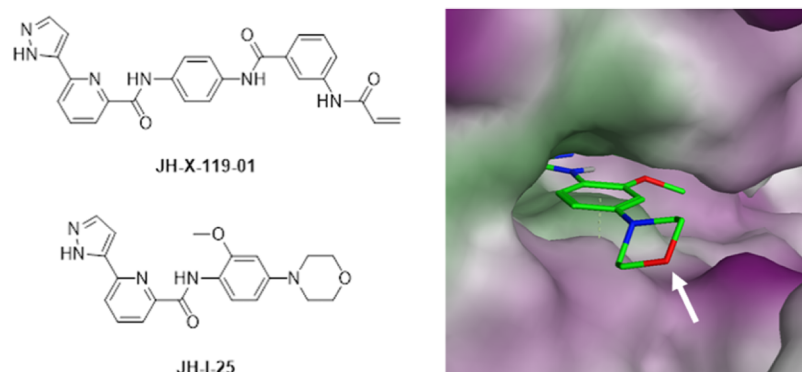


Figure 1. Chemical structures of the IRAK1 kinase inhibitors and the co-crystal structure of **JH-I-25** (green) with IRAK1 kinase (PDB: 6BFN). The linker attachment point is highlighted by the white arrow.

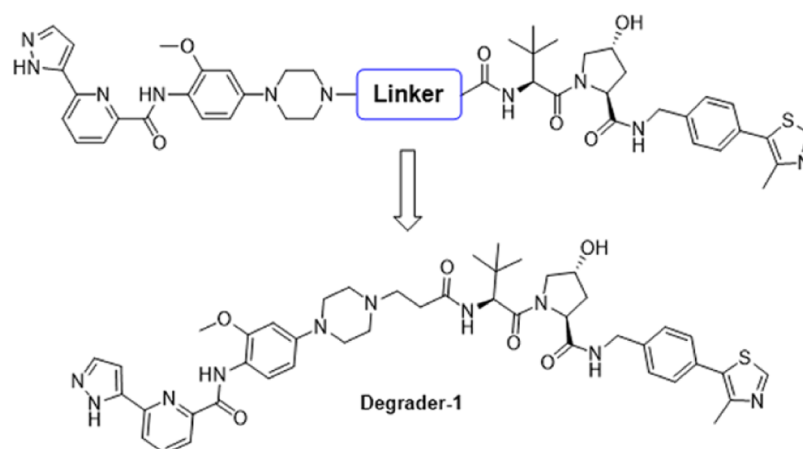


Figure 2. Design of IRAK1-targeting PROTACs and the chemical structure of **Degradar-1**.

results suggest that IRAK4 is dispensable for ABC DLBCL cell survival.⁵ On the other hand, genome-wide CRISPR screens pointed to IRAK1 as an essential gene for the survival of ABC DLBCL cells harboring MyD88 hotspot mutation.^{6,7} In a recent publication, Gray's group demonstrated the anti-proliferative activity of an IRAK1 covalent inhibitor in ABC DLBCL cell lines.⁸ Interestingly, this IRAK1 kinase inhibitor **JH-X-119-01** (Figure 1), which is very potent and selective in enzymatic assays (IRAK1 IC_{50} of 8 nM), only modestly inhibited the proliferation of ABC DLBCL cell lines with IC_{50} values in the micromolar range.⁸ These results suggested that kinase inhibition alone was not sufficient to fully disrupt myddosome signaling and effectively suppress lymphoma cell growth. We therefore hypothesize that the kinase-independent activities of IRAK1 are engaged and that the removal of the protein scaffold functions may be required to achieve maximal antagonism of the signaling pathway in MyD88 L265P mutant DLBCL cells.

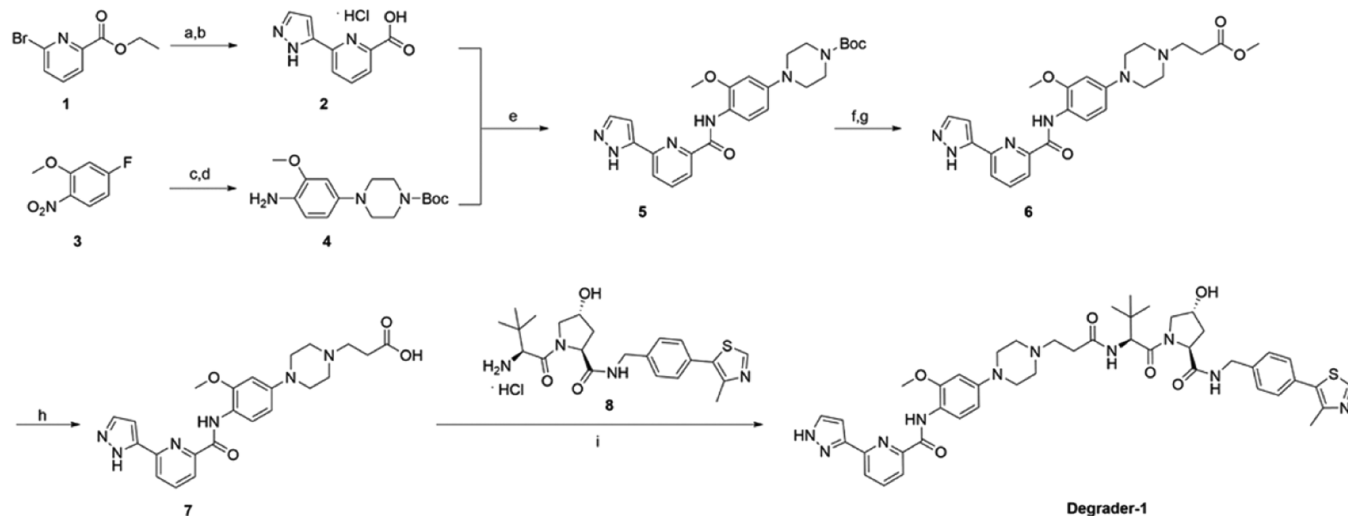
Here, we sought to eliminate the IRAK1 scaffolding function using bivalent chemical degraders. Degraders of this type, often represented as proteolysis targeting chimeras (PROTACs), are heterobifunctional small molecules that can induce degradation of a target protein by bringing it into proximity with an E3 ligase. When a ternary complex is formed, the E3 ligase ubiquitinates the target protein, leading to its proteasomal degradation.^{9–12} In this study, we report the design, synthesis, and biological evaluation of a series of IRAK1-targeting degraders. Several of these heterobifunctional molecules could efficiently and selectively degrade IRAK1 protein at

low concentrations, providing new pharmacological tools to probe for the IRAK1 scaffolding function. It was demonstrated that IRAK1 PROTACs effectively inhibited IRAK1 downstream signaling pathways and led to strong growth inhibition of MyD88-dependent ABC DLBCL cells.

RESULTS AND DISCUSSION

A set of published IRAK1 inhibitors were chosen as a starting point to develop IRAK1 PROTACs. Compound **JH-I-25** (Figure 1) was identified as a potent IRAK1/4 dual inhibitor with the first IRAK1 co-crystal structure (PDB: 6BFN) reported recently.^{13,14} This compound was also investigated to understand and verify its IRAK1 kinase inhibition activity. The crystal structure shows that the morpholine ring is in a solvent-exposed region, indicating a suitable site for linker attachment. Therefore, morpholine was replaced with piperazine to facilitate linker conjugation *via* amine alkylation (Figure 1).

For E3 ligase ligand selection, cereblon (CRBN) ligand thalidomide derivatives and the von Hippel–Lindau (VHL) ligand VH032 are the most frequently used ligands in PROTAC design.¹⁰ Previous studies indicated that thalidomide derivatives could potentially induce degradation of multiple neo-substrates, such as Ikaros (IKZF1), Aiolos (IKZF3), GSPT1, SALL4, and p63.^{15–18} Thalidomide derivatives that induce degradation of Ikaros and Aiolos could potentially lead to strong proliferation inhibition and apoptosis in ABC DLBCL cell lines, confounding the

Scheme 1. Synthesis of Degradator-1^a

^aReagents and conditions: (a) 1-(tetrahydro-2H-pyran-2-yl)-5-(4,4,5,5-tetramethyl-1,3,2-dioxaborolan-2-yl)-1H-pyrazole, Pd(dppf)Cl₂, Cs₂CO₃, dioxane/H₂O. (b) (i) NaOH, MeOH/H₂O. (ii) HCl, dioxane. (c) *tert*-Butyl piperazine-1-carboxylate, K₂CO₃, DMF. (d) H₂, Pd/C, MeOH. (e) HATU, TEA, DMF. (f) HCl, EtOAc. (g) Methyl 3-bromopropanoate, TEA, KI, NMP, microwave. (h) NaOH, THF/H₂O. (i) EDCI, HOBT, DIPEA, DMF.

Table 1. Biochemical and Protein Degradation Data of Degradator-1 and Warhead Compound JH-I-25

compounds	IRAK1 IC ₅₀ (nM) ^a	IRAK4 IC ₅₀ (nM) ^a	IRAK1 D _{max} (% of control) ^b	IRAK1 DC ₅₀ (nM) ^c
Degradator-1	80	368	88	134
JH-I-25	23	24	NA	NA

^aIRAK1 kinase inhibition potency (IC₅₀) determined by a Caliper biochemical assay. ^bMaximal IRAK1 and IRAK4 protein degradation (D_{max}) determined by immunoblotting 24 h after treatment. IRAK1 degradation was calculated from quantified Western blots. ^cDegradation potency (DC₅₀) of IRAK1 PROTACs determined by immunoblotting 24 h after treatment with degraders in the 293T cell line.

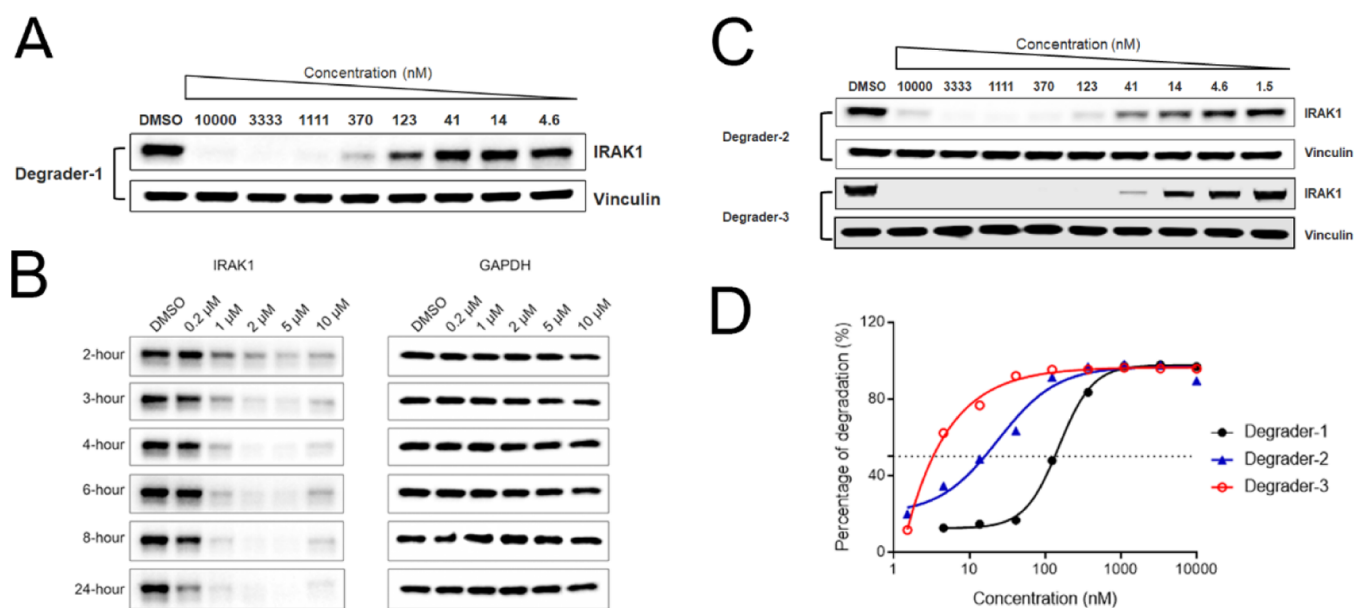
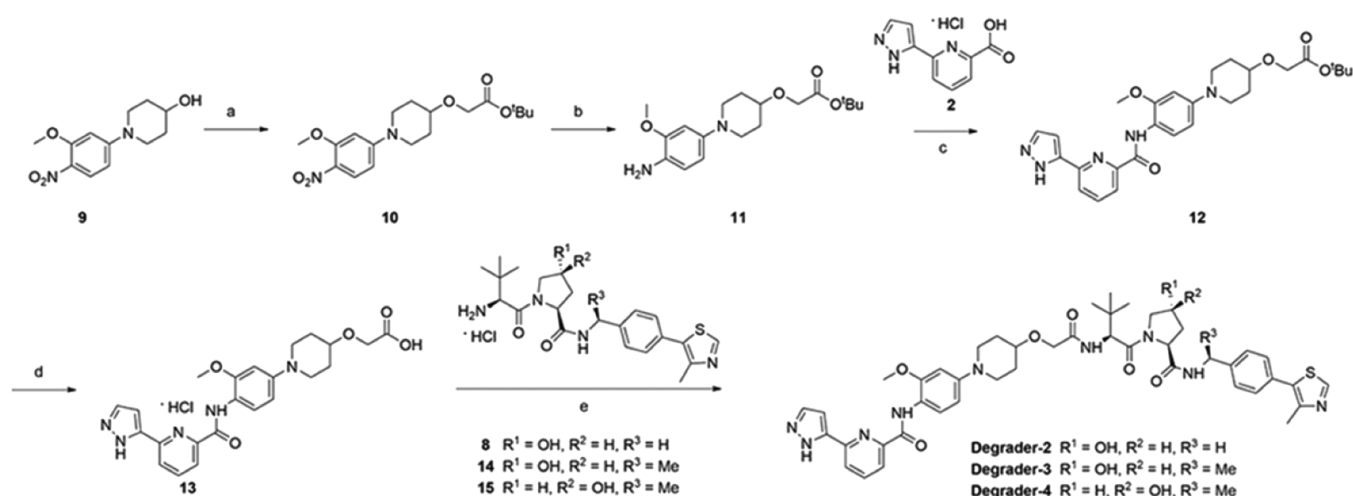


Figure 3. IRAK1 protein degradation profile in HEK293T cells for **Degradator-1**, **Degradator-2**, and **Degradator-3**. (A) Degradation effects of **Degradator-1** on IRAK1 proteins in HEK293T cells by Western blotting after 24 h treatment by **Degradator-1** at illustrated concentrations. (B) Characterization of **Degradator-1** for its concentration- and time-dependent IRAK1 protein degradation by Western blot analysis. (C) **Degradator-2** and **Degradator-3** dose-dependently degrades IRAK1 protein after 24 h incubation. (D) Quantitation of DC₅₀ values of **Degradator-1**, **Degradator-2**, and **Degradator-3** after 24 h incubation.

interpretation of IRAK1-dependent effects.¹⁹ To avoid potential off-target degradation from the CRBN E3 ligase and enable conclusive data for IRAK1 degradation validation,

the VHL E3 ligase ligand VH032 was selected for IRAK1 PROTAC design and connected to the anchor point of the piperazine ring moiety from the **JH-1-25** IRAK1 inhibitor *via*

Scheme 2. Synthesis of Degradator-2, Degradator-3, and Degradator-4^a

^aReagents and conditions: (a) *tert*-butyl 2-bromoacetate, NaH, THF; (b) Pd/C, H₂ (30 psi), MeOH; (c) HATU, DIPEA, DMF; (d) HCl (4 M in dioxane); and (e) EDCl, HOBT, DIPEA, DMF.

Table 2. Profiles of IRAK1 PROTACs with Different Linker Lengths and Compositions

compound	IRAK1 IC ₅₀ (nM) ^a	IRAK4 IC ₅₀ (nM) ^a	VHL FP IC ₅₀ (nM) ^b	IRAK1 D _{max} (% of control) ^c	IRAK1 DC ₅₀ (nM) ^d
Degradator-1	80	368	1646	88	134
Degradator-2	60	260	1400	95	16
Degradator-3 (JNJ-1013)	72	443	1071	96	3.3
Degradator-4	79	320	>10,000	18	>10,000
JH-I-25	23	24	NA	NA	NA

^aIRAK1 kinase inhibition potency (IC₅₀) determined by a Caliper biochemistry assay. ^bBinding affinity of degraders to VHL protein (IC₅₀) determined by an FP assay. ^cMaximal IRAK1 and IRAK4 protein degradation (D_{max}) determined by immunoblotting 24 h after treatment with degraders. ^dDegradation potency (DC₅₀) of IRAK1 degraders determined by immunoblotting 24 h after treatment.

different lengths and composition linkers (*e.g.*, alkyl linkers and polyethylene glycol linkers, Figure 2).^{20,21}

To generate the degrader compounds, a convergent synthesis method (Scheme 1) was developed to connect the piperazine group of the IRAK1 warhead with different linkers and a VHL amine intermediate (Figure 2).^{22,23} After library synthesis, the degradation potency (D_{max} and DC₅₀) of these PROTAC degraders was assessed by immunoblotting assays in HEK293T cells after 24 h of treatment. Interestingly, **Degradator-1** with the shortest linker (two methylene units) showed the most promising profile, demonstrating a DC₅₀ of 134 nM and a D_{max} of 88% at 10 μM (Table 1, Figures 2 and 3A). We also profiled the *in vitro* biochemical properties of both **Degradator-1** and **JH-I-25**. Table 1 summarizes the biochemical activity, determined by a Caliper kinase activity assay, of the designed PROTACs and the parent ligand to IRAK1 and IRAK4. The degrader molecule maintained a high-double-digit nM IRAK1 biochemical potency that was comparable to that of its parent compound **JH-I-25**, confirming the success of the rationally designed attachment vector. In an IRAK4 biochemical assay, however, the potency of compound **Degradator-1** dropped 15-fold, presumably because the front pocket of IRAK4 is largely occluded, while the front pocket of IRAK1 is open and accessible for binding.¹⁴ Interestingly, no IRAK4 protein degradation was observed with **Degradator-1** (Figure S4) even though it exhibited reasonable IRAK4 biochemical potency with an IC₅₀ of 368 nM. Despite the high sequence similarity (>90%) of IRAK1 and IRAK4 in their ATP binding pockets, significant degradation selectivity

for IRAK1 was achieved through heterobifunctional degraders over functional inhibition selectivity by **JH-I-25** and its degrader analogues. This suggests that the basis of degradation selectivity may reside in protein–protein interactions between the VHL E3 ubiquitin ligase and the targeted protein, that is, the ternary complex.²⁴ In other words, the engaged proteins may not lead to a productive ternary complex in the case of IRAK4. Independent experiments are in progress to confirm this hypothesis.

To evaluate the kinetics of IRAK1 degradation, we performed time course experiments in HEK293T cells by Western blot analysis using different concentrations of **Degradator-1**. Degradation occurred rapidly, with over 50% IRAK1 degradation achieved in 2 h across all ≥ 1 μM doses, and over 90% of protein degradation was achieved after 8 h (Figure 3B). At 10 μM, reduced degradation of the IRAK1 protein was observed, which is consistent with the “hook effect” commonly observed at high concentrations of PROTACs where individual binary complexes become saturated and compete for the formation of the E3 ligase–substrate–ligand ternary complex, causing the loss of degradation efficiency.²⁵

To our delight, through the replacement of the *N*-linked piperazine ring in the linker region of **Degradator-1** with an *O*-linked piperidine version (Scheme 2), the DC₅₀ of **Degradator-2** was improved to a low-double-digit nM range with a D_{max} of 95% (Table 2). Meanwhile, the addition of a methyl group in the *S*-configuration in the VHL binder moiety of **Degradator-2** yielded a 5-fold more potent compound, **Degradator-3** (JNJ-

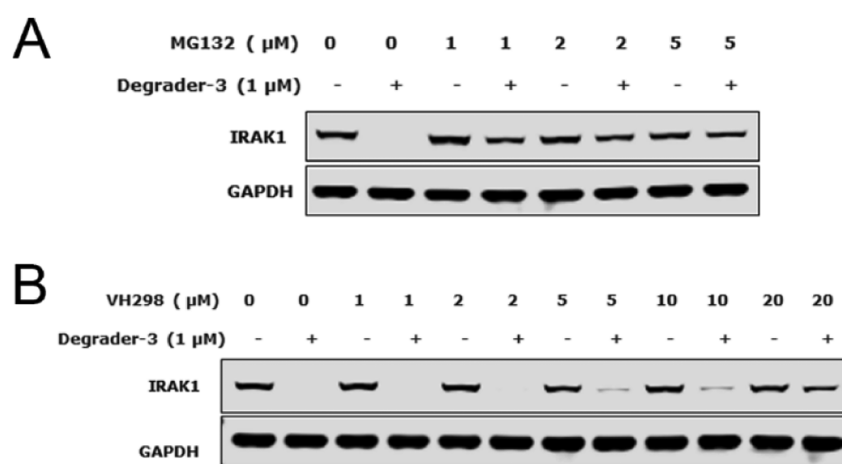


Figure 4. Mechanistic study of **Degradar-3** in HEK293T cells by Western blotting analysis. (A) **Degradar-3**-mediated IRAK1 degradation is abrogated by pretreatment with the proteasome inhibitor MG-132. (B) **Degradar-3**-mediated IRAK1 degradation is abrogated by pretreatment with the VHL ligand VH298.

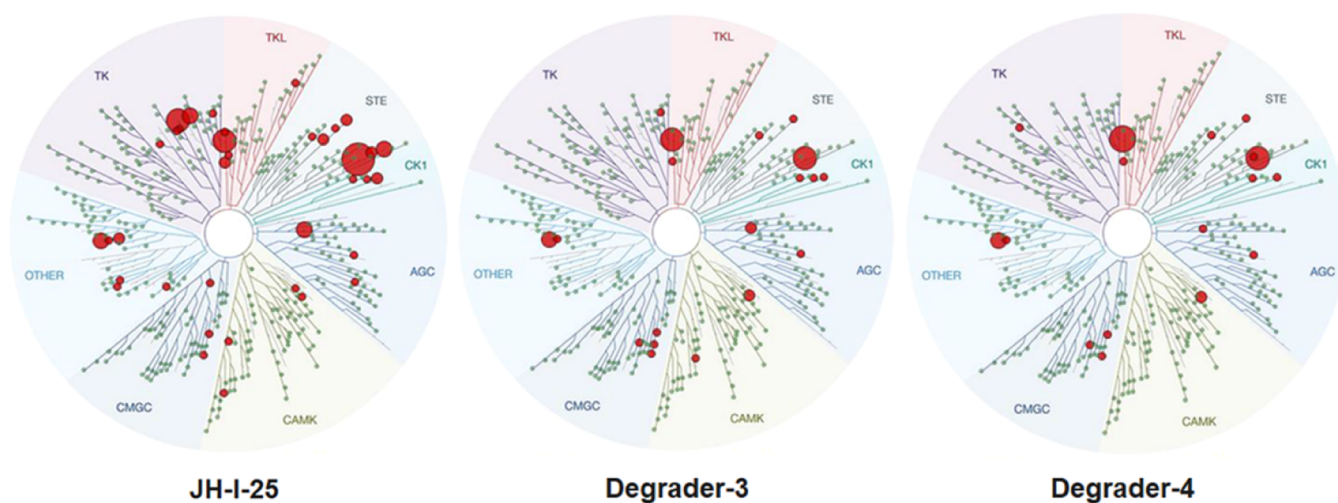


Figure 5. TREEspot interaction map of kinases for **JH-I-25**, **Degradar-3**, and **Degradar-4** from the KinomeScan competition binding assay profiled at 1 μM concentration.

1013, Table 2). Both PROTACs effectively degraded IRAK1 protein in a dose-dependent manner (Figure 3C,D). Interestingly, in a direct comparison, **Degradar-1**, **Degradar-2**, and **Degradar-3** did not exhibit distinct potency differences in IRAK1 biochemical activity or in the VHL fluorescence polarization (FP) binding assay (Table 2). This again indicates that there is no significant correlation between the binary binding potency and degradation potency. In addition, **Degradar-4**, the diastereoisomer of **Degradar-3** with an inverted hydroxyl stereocenter, was designed as a reference. As expected, **Degradar-4** lost the VHL binding affinity ($\text{IC}_{50} > 10 \mu\text{M}$ in a VHL FP assay) and did not show significant IRAK1 degradation activity ($\text{DC}_{50} > 10 \mu\text{M}$).

Next, **Degradar-3** was selected as a representative IRAK1 PROTAC for further evaluation. To verify that the degradation of IRAK1 protein was mediated through the ubiquitination and proteasome system, we utilized a proteasome inhibitor, MG-132, to disrupt proteasome function and a VHL ligand, VH298, to compete for VHL binding.²¹ As shown in Figure 4A,B, IRAK1 degradation was completely prevented by either the proteasome inhibitor MG-132 or competitive VHL ligand VH298, confirming that the degradation of IRAK1 protein is

through the proteasome mediated by the VHL E3 ubiquitin ligase.

To compare biochemical selectivity profiles, we submitted **JH-I-25**, **Degradar-3**, and **Degradar-4** for the KinomeScan competition binding assay panel (DiscoverX), which comprises 469 kinases. **JH-I-25** is a relatively selective IRAK1 inhibitor as a limited number of off-targets were inhibited at 1 μM , as shown in Figure 5. Both **Degradar-3** and **Degradar-4** degraders demonstrated higher selectivity toward IRAK1 compared to **JH-I-25** as fewer off-targets were inhibited in the KinomeScan assay. Conversion of **JH-I-25** into a PROTAC retained the IRAK1 binding but significantly reduced the binding affinity for the other members of the kinase superfamily that had been inhibited by **JH-I-25**. Compared to the 17 off-targets with more than 90% inhibition at 1 μM from **JH-I-25**, only 3 off-targets were identified for **Degradar-3** (BIKE, DRAK2, and YSK4). It is worth mentioning that the VHL epimer control compound **Degradar-4** showed an almost identical kinome profile to that of **Degradar-3**.

To determine the global proteome-wide degradation profiles of the IRAK1 degraders, an unbiased quantitative mass

spectrometry-based approach was employed. A GCB DLBCL cell line (Toledo) was selected due to sufficient expression of endogenous IRAK1 within this line, allowing simultaneous detection of IRAK1 loss with other key components of the NF- κ B machinery. In the experiment, Toledo cells were treated with either DMSO (control) or **Degrader-3** at 1 μ M for 6 h before the cell lysates were collected (Figure S1). Proteome-wide quantitative mass spectrometric analysis was then performed as described in the Supporting Information. Significance cutoff was set at a 1.5-fold change with a minimum of two unique peptide measurements and *p*-values of less than 0.05. In total, 7550 proteins were successfully quantified in this experiment, among which IRAK1, cyclin G-associated kinase (GAK), and NmrA-like family domain-containing protein 1 (NMRAL1) were the only three proteins which exhibited a significant decrease in abundance after **Degrader-3** treatment (Figure 6). The proteome analysis

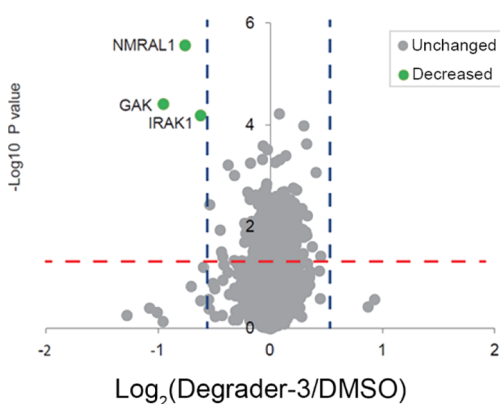


Figure 6. Volcano plots of abundance proteomics data of **Degrader-3** by proteomics analysis. Log fold change in abundance of protein with two unique peptide measurement using quantitative mass spectrometry after 6 h treatment of Toledo cells with 1 μ M **Degrader-3**.

showed that the degradation profile was far more selective than the kinase binding profile, where only the kinases IRAK1 and GAK were decreased, while the changes for other kinase off-targets were negligible. It is noteworthy to point out that similar proteomics assays were carried out in the ABC-DLBCL cell line HBL1, where low endogenous levels of IRAK1 were detectable only by Western blotting but were beyond the sensitivity of mass spectrometry. GAK and NMRAL1 proteins were also the only two off-targets which were observed after treatment of **Degrader-3** at 1 μ M for 6 h (Figure S2). Surprisingly, though **Degrader-3** did not exhibit a strong GAK binding affinity in the KinomeScan competition binding assay (63% inhibition at 1 μ M), it degraded GAK to 50% at 1 μ M after 6 h treatment in the quantitative mass spectroscopy experiment. Our efforts to confirm the finding is limited by the availability of a specific antibody. On the other hand, degradation of NMRAL1 by **Degrader-3** was reproduced in both HEK293T and HBL-1 cells by Western blotting (data not shown). The degradation mechanism for NMRAL1 is inconclusive since the protein is not a kinase, and degradation may be mediated through other mechanisms which are under further investigation. Consistent with the findings from the proteomics study, **Degrader-3** degraded only IRAK1, not IRAK4, as shown by Western blotting analysis (Figure S4). Collectively, the KinomeScan and proteomics data support

that **Degrader-3** acts as a potent and selective IRAK1 degrader.

Next, utilizing the highly selective IRAK1 PROTAC **Degrader-3** and its epimer control **Degrader-4**, we aimed to investigate the biological consequence of IRAK1 depletion in ABC DLBCL cell lines harboring MyD88 L265P mutation and dependent on the MyD88 signaling pathway for survival, such as HBL-1 and OCI-LY10. We initially evaluated the IRAK1 degradation effect by immunoblotting analysis after 24 h treatment with degrader compounds in both ABC DLBCL cell lines. Although **Degrader-3** demonstrated comparable IRAK1 degradation potency in HBL-1 cell lines compared to HEK293T cells with DC₅₀ values of 3.0 and 3.3 nM, respectively, a decreased degradation potency was observed in the OCI-LY10 cell line with a DC₅₀ of 20 nM (Figure 7A).

To evaluate the effects of IRAK1 depletion on the IRAK1 downstream signaling pathway in ABC DLBCL cell lines, HBL-1 cells were treated with **Degrader-3** and its epimer **Degrader-4** for 24 h before lysis and immunoblotting to detect phosphorylation events downstream of IRAK1 signaling. As shown in Figure 7B, **Degrader-3** resulted in a significant decrease in p-I κ B α and p-STAT3 and minimal changes in total STAT3 levels, consistent with the notion that oncogenic MyD88/IRAK signaling converges on NF- κ B activation and STAT3 phosphorylation and contributes to the survival of DLBCL cells.^{26,27} Not surprisingly, although the epimer control compound **Degrader-4** binds to the IRAK1 kinase domain with the same affinity (Table 2) and thus may act as an IRAK1 kinase inhibitor, it was unable to degrade IRAK1 at all doses tested. Minimal changes in cell signaling were observed by **Degrader-4**, supporting the hypothesis that the IRAK1 protein scaffolding function, as opposed to its kinase activity, is important in maintaining constitutive NF- κ B activation in ABC DLBCL cells.^{4,6}

We then evaluated the effects of targeted IRAK1 degradation on cellular apoptosis. Accordingly, a 24 h treatment of **Degrader-3** in HBL-1 cell lines increased apoptosis, as monitored by PARP cleavage in a Western blot assay. As expected, treatment with equivalent doses of **Degrader-4** did not induce IRAK1 protein degradation and produced no change in PARP cleavage (Figure 7C). These data suggest that the IRAK1 protein scaffolding function plays an important role in maintaining constitutive NF- κ B and STAT3 activation in ABC DLBCL cells.

Next, we sought to determine the effect of IRAK1 depletion on ABC DLBCL cell proliferation. HBL-1 and OCI-LY10 cells with MyD88 L265P mutation were treated with **Degrader-3** for 12 days, and cell viability was determined by CTG assays. In line with the requirement for VHL engagement, we also profiled the control epimer **Degrader-4**. In the HBL-1 cell line, **Degrader-3** exhibited significantly enhanced cytotoxicity as compared with **Degrader-4** (60 nM vs > 1.5 μ M); similar trends were observed in OCI-LY10 cell lines (170 nM vs > 3 μ M) (Figure 7D). In contrast, **JH-I-25**, a dual kinase inhibitor of IRAK1 and IRAK4, showed marginal cell growth inhibition in HBL1 with an IC₅₀ of 2.8 μ M (Figure S3). The results demonstrate the distinct advantage of IRAK1 degradation over kinase inhibition as the degrader showed significantly improved anti-proliferative effects (over 40-fold) compared to the kinase inhibitor in HBL-1. Taken together, these data suggest that the IRAK1 scaffolding function, rather than its kinase activity, is required for ABC DLBCL cell survival and proliferation.

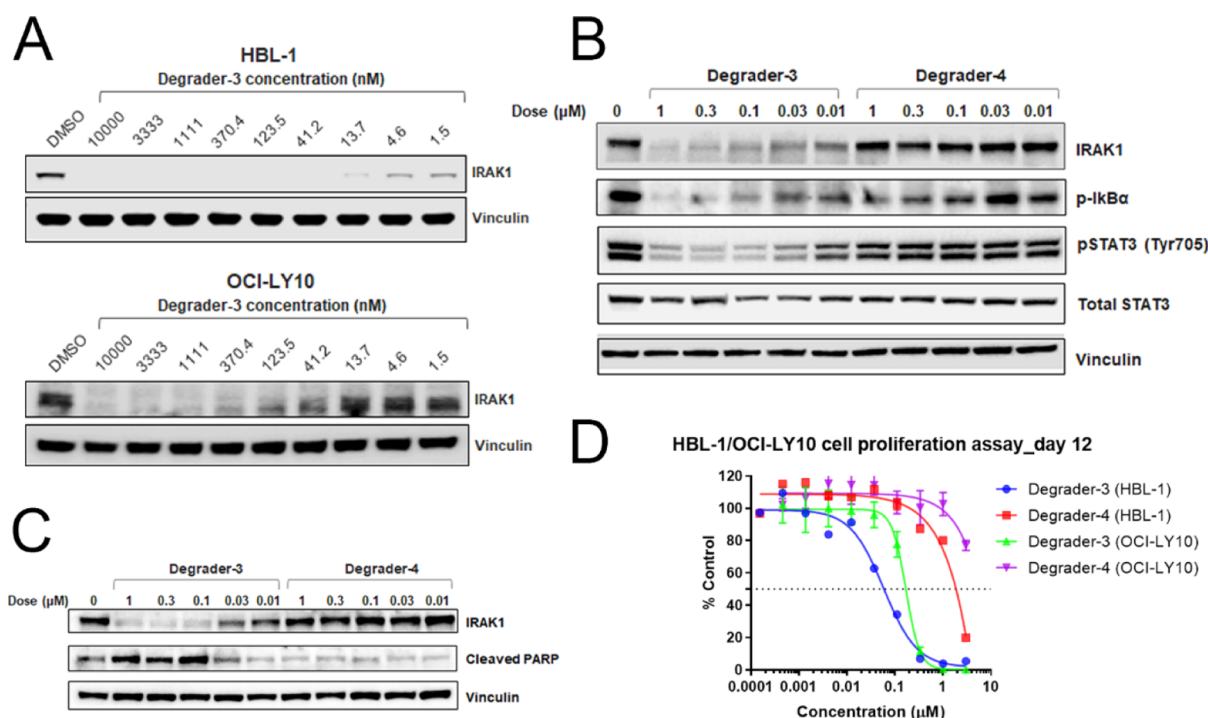


Figure 7. Characterization of **Degrader-3** and **Degrader-4** in ABC DLBCL cell lines. (A) DLBCL cell lines were treated with **Degrader-3** at the indicated concentrations for 24 h. IRAK1 protein levels were determined by Western blotting. (B) HBL-1 cells were treated with **Degrader-3** or its epimer **Degrader-4** at the indicated doses for 24 h. Phosphorylated I κ B α and STAT3 protein levels were determined by Western blotting. (C) Cleaved PARP was determined by Western blotting. (D) Cell proliferative assay in HBL-1 and OCI-LY10 cells with MyD88 mutation.

CONCLUSIONS

We have discovered a novel series of VHL E3 ligase-based IRAK1 PROTAC degraders. One of the most potent compounds, **Degrader-3** (**JNJ-1013**), effectively degrades IRAK1 with a DC_{50} of 3 nM in HBL-1 cells. In ABC DLBCL cell lines with MyD88 L265P mutation, **JNJ-1013** potently inhibits IRAK1 downstream signaling pathways, induces apoptosis, and demonstrates strong anti-proliferative effects, suggesting a critical role for the IRAK1 scaffolding function in ABC DLBCL cell survival. This class of highly selective IRAK1 degraders offers a pharmacological approach to evaluate the biological roles of IRAK1 beyond its enzymatic activity in various disease indications.

EXPERIMENTAL SECTION

Chemistry. All commercially obtained solvents and reagents were used as received. All solvents used for chemical reactions were of anhydrous grade, unless specifically indicated. Structures of the target compounds in this work were assigned by the use of NMR spectroscopy and mass spectroscopy (MS). The purities of all non-salt compounds were >95%, as determined on an Agilent 1200 HPLC system, an XTerra 3.5 μ m 4.6 \times 150 mm MS C18 column, using 0.04 (v/v) TFA in water and 0.02 (v/v) TFA in acetonitrile as the mobile phase. 1 H NMR spectra were recorded on a Bruker ADVANCE III (400 MHz) or a Varian 400MR (400 MHz) NMR spectrometer. Chemical shifts are reported in parts per million (ppm, δ) using the residual solvent line as an internal reference. Splitting patterns are reported as s (singlet), d (doublet), t (triplet), q (quartet), m (multiplet), br m (broad multiplet), or br s (broad singlet). Coupling constants (J) are reported in Hertz (Hz). Mass spectrometric analyses for nucleosides were performed on an Agilent 1200 HPLC system with an Agilent 6110/6140/1956C MSD mass spectrometer using ESI as ionization, a Phenomenex Luna C18 5 μ m 5.0 \times 20 mm column, mobile phase: 0.04%(v/v) TFA in water and 0.02%(v/v) TFA in acetonitrile, 40 $^{\circ}$ C, and a flow rate of 0.4 mL/min. Unless

specifically indicated, chromatography refers to flash chromatography on a silica gel column.

6-(1H-Pyrazol-5-yl)picolinic Acid Hydrochloride (2). Step 1: Ethyl 6-bromopicolinate (**1**) (15.0 g, 65.2 mmol), 1-(tetrahydro-2H-pyran-2-yl)-5-(4,4,5,5-tetramethyl-1,3,2-dioxaborolan-2-yl)-1H-pyrazole (19.9 g, 71.5 mmol), and cesium carbonate (63.7 g, 196 mmol) in 1,4-dioxane (200 mL) and H $_2$ O (50 mL) were added to a 500 mL round-bottomed flask. The mixture was sparged with nitrogen three times and then treated with Pd(dppf)Cl $_2$ (3.62 g, 6.53 mmol). Then, the mixture was sparged with nitrogen three times and heated to 90 $^{\circ}$ C for 16 h. The reaction mixture was filtered and diluted with ethyl acetate (100 mL). The aqueous solution was acidified to pH = 5–6 by citric acid, extracted with dichloromethane (100 mL \times 5), washed with brine, and dried over Na $_2$ SO $_4$. The organic layer was filtered and concentrated under reduced pressure to give the title compound as a gray solid (15.0 g, 76%). LCMS (ESI $^+$): calcd for C $_{16}$ H $_{19}$ N $_3$ O $_3$ = 301.1, found; [M + H] $^+$ = 302.2, t_R = 1.10 min.

Step 2: Ethyl 6-(1-(tetrahydro-2H-pyran-2-yl)-1H-pyrazol-5-yl)picolinate (15.0 g, 49.8 mmol) and NaOH (2.39 g, 59.8 mmol) in MeOH (45 mL) and H $_2$ O (45 mL) were added to a 250 mL round-bottomed flask. The mixture was stirred at 20 $^{\circ}$ C for 2 h. The reaction mixture was concentrated, and the residue was diluted with H $_2$ O (50 mL). The mixture was acidified to pH = 5–6 by citric acid, extracted with dichloromethane (100 mL \times 5), washed with brine, and dried over Na $_2$ SO $_4$. The organic layer was filtered and concentrated under reduced pressure to give 6-(1-(tetrahydro-2H-pyran-2-yl)-1H-pyrazol-5-yl)picolinic acid (12.0 g, 75.0%) as a gray solid. The crude product was then dissolved in dichloromethane (20 mL) and HCl/dioxane (50 mL, 4 M) and added to a 250 mL round-bottomed flask. The reaction mixture was stirred at 25 $^{\circ}$ C for 1 h. Then, the mixture was filtered, and the filter cake was dried to give the title product as a white solid (9.8 g, 98.3%). 1 H NMR (400 MHz, DMSO- d_6): δ 10.67 (br s, 2H), 8.17 (dd, J = 0.8, 7.6 Hz, 1H), 8.05 (t, J = 7.6 Hz, 1H), 7.99–7.94 (m, 1H), 7.81 (d, J = 2.0 Hz, 1H), 7.01 (d, J = 2.0 Hz, 1H). LCMS (ESI $^+$) calcd for C $_9$ H $_7$ N $_3$ O $_2$ = 189.0, found; [M + H] $^+$ = 189.9, t_R = 0.84 min.

tert-Butyl 4-(4-amino-3-methoxyphenyl)piperazine-1-carboxylate (4). Step 1: 4-Fluoro-2-methoxy-1-nitrobenzene (3) (10.0 g, 58.4 mmol), *tert*-butyl piperazine-1-carboxylate (11.4 g, 61.2 mmol), potassium carbonate (20.2 g, 87.7 mmol), and DMF (80 mL) were added to a 250 mL round-bottomed flask. The reaction mixture was stirred at 80 °C for 16 h. The reaction mixture was poured into 150 mL water and stirred at 25 °C for 0.5 h. The mixture was filtered, the cake was washed with petroleum ether (60 mL × 2), and the resultant mixture was concentrated to dryness under reduced pressure to afford the desired product as a yellow solid (19.0 g, 91.2%). ¹H NMR (400 MHz, DMSO-*d*₆): δ 7.89–7.82 (m, 1H), 6.58–6.51 (m, 1H), 6.50–6.45 (m, 1H), 3.87 (s, 3H), 3.45–3.40 (m, 8H), 1.38 (s, 9H). LCMS (ESI⁺): calcd for C₁₆H₂₃N₃O₅ = 337.2, found; [M + H]⁺ = 338.1, *t*_R = 0.88 min.

Step 2: *tert*-Butyl 4-(3-methoxy-4-nitrophenyl)piperazine-1-carboxylate (56.0 g, 166 mmol), wet Pd/C (5.00 g, 10% on activated carbon), and MeOH (1 L) were added to a 2 L reaction flask. The suspension was degassed under vacuum and purged with H₂ three times. The mixture was stirred under H₂ (30 psi) at 25 °C for 12 h. The mixture was filtered through a pad of celite, and the filter cake was washed with MeOH (50 mL). The filtrate was evaporated to dryness to give the title compound as a purple solid (55.0 g, 97.0%). ¹H NMR (400 MHz, DMSO-*d*₆): δ 6.57–6.47 (m, 2H), 6.35–6.26 (m, 1H), 4.51–4.10 (m, 2H), 3.74 (s, 3H), 3.50–3.39 (m, 4H), 2.93–2.81 (m, 4H), 1.41 (s, 9H). LCMS (ESI⁺): calcd for C₁₆H₂₃N₃O₃ = 307.2, found; [M + H]⁺ = 308.3, *t*_R = 0.74 min.

tert-Butyl 4-(4-(6-(1H-pyrazol-5-yl)picolinamido)-3-methoxyphenyl)piperazine-1-carboxylate (5). A solution of *tert*-butyl 4-(4-amino-3-methoxyphenyl)piperazine-1-carboxylate (4) (10.0 g, 32.5 mmol), 6-(1H-pyrazol-5-yl)picolinic acid hydrochloride (2) (6.15 g, 32.5 mmol), HATU (14.8 g, 38.9 mmol), and TEA (13.6 mL, 97.6 mmol) in DMF (100 mL) was stirred at 25 °C for 8 h. The reaction mixture was diluted with water (200 mL), extracted with ethyl acetate (300 mL × 2), washed with brine (200 mL × 3), and dried over Na₂SO₄. The organic layer was filtered and concentrated under reduced pressure to give a crude product, which was purified by chromatography on silica gel (eluent—petroleum ether:ethyl acetate = 1:0 to 0:1) to give the title compound as a gray solid (11.0 g, 70.7%). ¹H NMR (400 MHz, DMSO-*d*₆): δ 13.94–13.17 (m, 1H), 10.65–10.36 (m, 1H), 8.29–8.18 (m, 1H), 8.14–8.00 (m, 2H), 7.94 (s, 1H), 7.67–7.57 (m, 1H), 7.04–6.96 (m, 1H), 6.79–6.71 (m, 1H), 6.61–6.55 (m, 1H), 3.99 (s, 2H), 3.86 (s, 1H), 3.48 (br s, 4H), 3.13 (d, *J* = 4.5 Hz, 4H), 1.43 (s, 9H). LCMS (ESI⁺): calcd for C₂₅H₃₀N₆O₄ = 478.2, found; [M + H]⁺ = 479.1, *t*_R = 0.925 min.

Methyl 3-(4-(4-(6-(1H-pyrazol-5-yl)picolinamido)-3-methoxyphenyl)piperazin-1-yl)propanoate (6). Step 1: *tert*-Butyl 4-(4-(6-(1H-pyrazol-5-yl)picolinamido)-3-methoxyphenyl)piperazine-1-carboxylate (8.50 g, 17.8 mmol) and HCl in EtOAc (80 mL, 4 M) were added to a 250 mL round-bottomed flask. The reaction mixture was stirred at room temperature for 2 h. The mixture was concentrated under reduced pressure to give the title compound as a white solid (7.00 g, 93.9%). ¹H NMR (400 MHz, DMSO-*d*₆): δ 10.58 (s, 1H), 9.68–9.31 (m, 2H), 8.20–8.00 (m, 4H), 7.91–7.85 (m, 1H), 7.00 (s, 1H), 6.87–6.80 (m, 1H), 6.69–6.63 (m, 1H), 3.96 (s, 3H), 3.53–3.39 (m, 4H), 3.32–3.12 (m, 4H). LCMS (ESI⁺): calcd for C₂₀H₂₂N₆O₂ = 378.2, found; [M + H]⁺ = 379.2, *t*_R = 0.69 min.

Step 2: Methyl 3-bromopropanoate (100 mg, 0.599 mmol), *N*-(2-methoxy-4-(piperidin-4-yl)phenyl)-6-(1H-pyrazol-5-yl)picolinamide hydrochloride (249 mg, 0.600 mmol), triethylamine (0.8 mL, 5.74 mmol), potassium iodide (99.0 mg, 0.596 mmol), and 1-methyl-2-pyrrolidinone (2 mL) were added to a 10 mL sealed tube. The mixture was heated and stirred at 100 °C under a microwave initiator for 2 h. The mixture was then poured into water (10 mL) and extracted with ethyl acetate (20 mL × 2). The organic extracts were dried over anhydrous Na₂SO₄, filtered, and concentrated under reduced pressure to afford the crude product, which was purified by chromatography on silica gel (eluent—dichloromethane:methanol = 1:0 to 10:1) to afford the title product as a brown oil (150 mg, 48.5%). LCMS (ESI⁺): calcd for C₂₄H₂₈N₆O₄ = 464.2, found; [M +

H]⁺ = 465.2, *t*_R = 0.67 min. ¹H NMR (400 MHz, DMSO-*d*₆): δ = 13.88–13.23 (br s, 1H), 10.58–10.40 (br s, 1H), 8.30–7.45 (m, 5H), 7.06–6.91 (m, 1H), 6.78–6.63 (m, 1H), 6.54 (d, *J* = 8.8 Hz, 1H), 4.02–3.82 (m, 3H), 3.61 (s, 3H), 3.18–3.12 (m, 4H), 2.66–2.59 (m, 2H), 2.54 (d, *J* = 6.1 Hz, 4H), 2.20–2.16 (m, 2H).

3-(4-(4-(6-(1H-pyrazol-5-yl)picolinamido)-3-methoxyphenyl)piperazin-1-yl)propanoic Acid (7). Methyl 3-(4-(4-(6-(1H-pyrazol-5-yl)picolinamido)-3-methoxyphenyl)piperidin-1-yl)propanoate (6) (150 mg, 0.323 mmol), aqueous NaOH (6 mL, 1 M), and THF (3 mL) were added to a 50 mL round-bottomed flask. The reaction mixture was stirred at 20 °C for 1 h. The reaction mixture was concentrated with pH adjusted to 6–7 with aqueous HCl (1 M), and a pale-yellow precipitate was formed. The precipitate was filtrated and dried to give the title product as a yellow solid (120 mg, 82.5%). LCMS (ESI⁺): calcd for C₂₃H₂₆N₆O₄ = 450.2, found; [M + H]⁺ = 451.0, *t*_R = 0.77 min. ¹H NMR (400 MHz, DMSO-*d*₆): δ = 13.83–12.25 (m, 1H), 10.70–10.42 (m, 1H), 8.23–7.98 (m, 4H), 7.92–7.79 (m, 1H), 7.02–6.96 (m, 1H), 6.84–6.77 (m, 1H), 6.65–6.57 (m, 1H), 4.06–3.92 (m, 3H), 3.35–3.03 (m, 11H), 2.93–2.78 (m, 2H).

(2S,4R)-1-((S)-2-Amino-3,3-dimethylbutanoyl)-4-hydroxy-N-(4-(4-methylthiazol-5-yl)benzyl)pyrrolidine-2-carboxamide Hydrochloride (8). The free amine compound was prepared according to the procedure published.²⁸ *tert*-Butyl ((S)-1-((2S,4R)-4-hydroxy-2-((4-(4-methylthiazol-5-yl)benzyl)carbamoyl)pyrrolidin-1-yl)-3,3-dimethyl-1-oxobutan-2-yl)carbamate (1.00 g, 1.88 mmol) and 4 M HCl in dioxane (8 mL) were added into a 50 mL round-bottomed flask. The mixture was stirred at 25 °C for 30 min. The reaction mixture was concentrated to dryness under reduced pressure to afford the title product as a pale white solid (880 mg, crude). Data match the previous reports.

N-(4-(4-(3-(((S)-1-((2S,4R)-4-Hydroxy-2-((4-(4-methylthiazol-5-yl)benzyl)carbamoyl)pyrrolidin-1-yl)-3,3-dimethyl-1-oxobutan-2-yl)amino)-3-oxopropyl)piperazin-1-yl)-2-methoxyphenyl)-6-(1H-pyrazol-3-yl)picolinamide (Degradate-1). 3-(4-(6-(1H-pyrazol-3-yl)picolinamido)-3-methoxyphenyl)piperazin-1-yl)propanoic acid (7) (100 mg, 0.212 mmol), 1-hydroxybenzotriazole (43.0 mg, 0.318 mmol), *N*-ethyl-*N*-isopropylpropan-2-amine (138 mg, 1.07 mmol), 1-(3-dimethylaminopropyl)-3-ethylcarbodiimide hydrochloride (61.0 mg, 0.318 mmol), and DMF (3 mL) were added to a 50 mL round-bottomed flask. (2S,4R)-1-((S)-2-Amino-3,3-dimethylbutanoyl)-4-hydroxy-*N*-(4-(4-methylthiazol-5-yl)benzyl)pyrrolidine-2-carboxamide-HCl (8) (99.0 mg, 0.212 mmol) was added to the mixture. The reaction mixture was stirred at room temperature for 8 h. The mixture was then poured into water (8 mL) and extracted with ethyl acetate (15 mL × 2). The organic extracts were washed with brine (8 mL), dried over anhydrous Na₂SO₄, filtered, and concentrated under reduced pressure to afford the crude product, which was purified by prep-TLC (dichloromethane:methanol = 10:1, *R*_f = 0.4) to afford the title product as a yellow powder (50.2 mg, 27.1% yield). ¹H NMR (400 MHz, DMSO-*d*₆): δ 13.90 (br s, 0.3H), 13.24 (br s, 0.7H), 10.66–10.21 (m, 1H), 9.02–8.87 (m, 1H), 8.73–8.43 (m, 2H), 8.32–7.51 (m, 5H), 7.48–7.27 (m, 4H), 7.07–6.90 (m, 1H), 6.81–6.62 (m, 1H), 6.58–6.46 (m, 1H), 5.17 (d, *J* = 3.4 Hz, 1H), 4.58 (d, *J* = 9.5 Hz, 1H), 4.50–4.32 (m, 3H), 4.28–4.16 (m, 1H), 4.03–3.77 (m, 3H), 3.72–3.59 (m, 2H), 3.31–3.14 (m, 4H), 2.71–2.53 (m, 6H), 2.49–2.44 (m, 1H), 2.40 (s, 3H), 2.37–2.29 (m, 1H), 2.07–2.00 (m, 1H), 1.96–1.87 (m, 1H), 0.96 (s, 9H). ¹³C NMR (100 MHz, DMSO-*d*₆): δ 172.5, 171.4, 170.1, 160.9, 151.7, 151.6, 150.4, 149.9, 149.5, 148.7, 148.1, 139.9, 139.5, 131.6, 130.9, 130.1, 129.1, 128.5, 127.8, 122.4, 120.5, 120.0, 119.6, 107.2, 103.5, 100.1, 69.4, 59.2, 56.9, 56.7, 56.6, 54.5, 52.8, 48.9, 42.1, 40.6, 38.4, 35.9, 32.8, 26.9, 16.4. LCMS (ESI⁺): calcd for C₄₅H₅₄N₁₀O₆S = 862.4, found; [M + H]⁺ = 863.4, *t*_R = 0.4 min. HRMS (ESI): *m/z* [M + H]⁺ Calcd for C₄₅H₅₄N₁₀O₆S, 863.4027; found, 863.4036.

tert-Butyl 2-((1-(3-methoxy-4-nitrophenyl)piperidin-4-yl)-oxy)acetate (10). 1-(3-Methoxy-4-nitrophenyl)piperidin-4-ol (500 mg, 1.98 mmol) (9) and THF (20 mL) were added to a 50 mL round-bottomed flask at 0 °C before being treated with sodium hydride (119 mg, 2.97 mmol), and the mixture was stirred at 0 °C for

5 min. The reaction mixture was treated with *tert*-butyl 2-bromoacetate (770 mg, 3.96 mmol) at 0 °C, warmed, and stirred at 25 °C for 16 h. Brine (10 mL) was added to the mixture, and the mixture was concentrated under reduced pressure to remove THF before being diluted with H₂O (10 mL); then, the mixture was extracted with EtOAc (30 mL × 3). The combined organic extracts were dried over anhydrous Na₂SO₄, filtered, and concentrated to dryness under reduced pressure to give the crude product, which was purified by chromatography on silica gel (eluent—petroleum ether:ethyl acetate = 100:0 to 1:1) to afford the desired compound as a brown oil (650 mg, 76%). ¹H NMR (400 MHz, DMSO-*d*₆): δ 7.87 (d, *J* = 9.6 Hz, 1H), 6.59 (dd, *J* = 2.4, 9.2 Hz, 1H), 6.52–6.49 (m, 1H), 4.05 (s, 2H), 3.90 (s, 3H), 3.81–3.73 (m, 2H), 3.66–3.59 (m, 1H), 3.28–3.19 (m, 2H), 1.95–1.86 (m, 2H), 1.56–1.46 (m, 2H), 1.43 (s, 9H).

***tert*-Butyl 2-((1-(4-Amino-3-methoxyphenyl)piperidin-4-yl)oxy)acetate (11).** *tert*-Butyl 2-((1-(3-methoxy-4-nitrophenyl)piperidin-4-yl)oxy)acetate (10) (650 mg, 1.77 mmol), wet Pd/C (200 mg), and MeOH (20 mL) were added to a hydrogenation bottle under a N₂ atmosphere. The suspension was degassed under vacuum, purged with N₂ three times, and then purged with hydrogen another three times. The resulting mixture was stirred under hydrogen (30 psi) at 25 °C for 16 h. The mixture was filtered through a pad of celite, and the filter cake was washed with methanol (30 mL × 3). The combined filtrates were concentrated under reduced pressure to give the product as a brown oil (450 mg, 64%). ¹H NMR (400 MHz, DMSO-*d*₆): δ 6.52–6.47 (m, 2H), 6.31–6.26 (m, 1H), 4.26–4.13 (m, 2H), 4.01 (s, 2H), 3.73 (s, 3H), 3.45–3.40 (m, 1H), 3.27–3.21 (m, 2H), 2.68–2.61 (m, 2H), 1.92 (m, 2H), 1.60–1.51 (m, 2H), 1.43 (s, 9H). LCMS (ESI⁺): calcd for C₁₈H₂₈N₂O₄ = 336.2, found; [M + H]⁺ = 337.2, *t*_R = 0.70 min.

***tert*-Butyl 2-((1-(4-(6-(1H-pyrazol-5-yl)picolinamido)-3-methoxyphenyl)piperidin-4-yl)oxy)acetate (12).** *tert*-Butyl 2-((1-(4-amino-3-methoxyphenyl)piperidin-4-yl)oxy)acetate (11) (250 mg, 0.743 mmol), 6-(1H-pyrazol-5-yl)picolinic acid hydrochloride (2) (140 mg, 0.740 mmol), HATU (171 mg, 0.892 mmol), DIPEA (301 mg, 2.23 mmol), and DMF (3 mL) were added to a 10 mL round-bottomed flask. The reaction mixture was stirred at 25 °C for 2 h. The reaction mixture was concentrated under reduced pressure to obtain a residue, which was diluted with water (30 mL) and extracted with ethyl acetate (50 mL × 3). The combined organic layer was dried over anhydrous Na₂SO₄, filtered, and concentrated to dryness under reduced pressure to afford the crude product, which was purified by chromatography on silica gel (eluent—petroleum ether:ethyl acetate = 1:4 to 1:2) to give the desired product as a brown–green oil (216 mg, 57%). ¹H NMR (400 MHz, DMSO-*d*₆): δ 13.12 (s, 1H), 10.44 (s, 1H), 8.09–7.71 (m, 5H), 6.89 (d, *J* = 2.0 Hz, 1H), 6.62 (d, *J* = 2.0 Hz, 1H), 6.46 (dd, *J* = 2.4, 8.8 Hz, 1H), 4.02–3.90 (m, 2H), 3.85 (s, 3H), 3.43 (td, *J* = 4.2, 8.3 Hz, 2H), 2.87–2.73 (m, 3H), 1.93–1.80 (m, 2H), 1.53–1.42 (m, 2H), 1.34 (s, 9H). LCMS (ESI⁺): calcd for C₂₇H₃₃N₅O₅ = 507.2, found, [M + H]⁺ = 508.2, *t*_R = 0.85 min.

2-((1-(4-(6-(1H-Pyrazol-5-yl)picolinamido)-3-methoxyphenyl)piperidin-4-yl)oxy)acetic Acid Hydrochloride (13). *tert*-Butyl 2-((1-(4-(6-(1H-pyrazol-5-yl)picolinamido)-3-methoxyphenyl)piperidin-4-yl)oxy)acetate (12) (210 mg, 0.414 mmol) and HCl (4 mL, 4 M in dioxane) were added to a 50 mL round-bottomed flask. The resultant mixture was stirred at 25 °C for 2 h and then concentrated to dryness under reduced pressure to afford the title product as a white solid. (250 mg, crude). ¹H NMR (400 MHz, DMSO-*d*₆): δ 13.19–12.79 (br m, 2H), 10.53 (s, 1H), 8.18–8.12 (m, 1H), 8.12–7.98 (m, 3H), 7.90–7.81 (m, 1H), 6.99 (d, *J* = 2.0 Hz, 1H), 6.72 (d, *J* = 2.0 Hz, 1H), 6.55 (dd, *J* = 2.0, 8.8 Hz, 1H), 4.08 (s, 2H), 3.94 (s, 3H), 3.60–3.48 (m, 3H), 2.94–2.82 (m, 2H), 2.02–1.91 (m, 2H), 1.63–1.52 (m, 2H). LCMS (ESI⁺): calcd for C₂₃H₂₅N₅O₅ = 451.2, found, [M + H]⁺ = 452.2, *t*_R = 2.11 min.

(2S,4R)-1-((S)-2-Amino-3,3-dimethylbutanoyl)-4-hydroxy-N-((S)-1-(4-(4-methylthiazol-5-yl)phenyl)ethyl)pyrrolidine-2-carboxamide (14) and Epimer (2S,4S)-1-((S)-2-Amino-3,3-dimethylbutanoyl)-4-hydroxy-N-((S)-1-(4-(4-methylthiazol-5-yl)phenyl)ethyl)pyrrolidine-2-carboxamide (15). The compound

was prepared according to the procedure of *J. Med. Chem.* 2019, 62, 1420–1442. Data matched previous reports.

N-(4-(4-((S)-1-((2S,4R)-4-Hydroxy-2-((4-(4-methylthiazol-5-yl)benzyl)carbamoyl)pyrrolidin-1-yl)-3,3-dimethyl-1-oxobutan-2-yl)amino)-2-oxoethoxy)piperidin-1-yl)-2-methoxyphenyl)-6-(1H-pyrazol-5-yl)picolinamide (Degrader-2). 2-((1-(4-(6-(1H-pyrazol-5-yl)picolinamido)-3-methoxyphenyl)piperidin-4-yl)oxy)acetic acid hydrochloride (13) (100 mg, 0.205 mmol), (2S,4R)-1-((S)-2-amino-3,3-dimethylbutanoyl)-4-hydroxy-N-(4-(4-methylthiazol-5-yl)benzyl)pyrrolidine-2-carboxamide hydrochloride (8) (95.7 mg, 0.205 mmol), 1-hydroxybenzotriazole (41.5 mg, 0.307 mmol), DIPEA (79.5 mg, 0.615 mmol), and DMF (2 mL) were added to a 50 mL round-bottomed flask. Then, 1-(3-dimethylamino-propyl)-3-ethylcarbodiimide hydrochloride (58.9 mg, 0.307 mmol) was added to the mixture. The reaction mixture was stirred at 40 °C for 2 h. The mixture was purified by prep-HPLC (Column: Agela Durashell C18 150*25 5 μm, mobile phase A: water (10 mM NH₄HCO₃)-ACN, mobile phase B: acetonitrile, flow rate: 25 mL/min, gradient condition from 30% B to 60%). The pure fractions were collected, and the solvent was evaporated under vacuum to give a residue, which was lyophilized to give the title product as a yellow powder (20.7 mg, 11.7%). ¹H NMR (400 MHz, DMSO-*d*₆): δ 13.87 (br s, 0.3H), 13.22 (br s, 0.8H), 10.66–10.30 (m, 1H), 9.03–8.92 (m, 1H), 8.77–8.55 (m, 1H), 8.23–7.92 (m, 4H), 7.68–7.17 (m, 6H), 7.04–6.93 (m, 1H), 6.78–6.65 (m, 1H), 6.60–6.49 (m, 1H), 5.17 (d, *J* = 3.2 Hz, 1H), 4.56 (d, *J* = 9.5 Hz, 1H), 4.49–4.21 (m, 4H), 4.09–3.91 (m, 4H), 3.84 (br s, 1H), 3.73–3.46 (m, 5H), 3.04–2.85 (m, 2H), 2.47–2.40 (m, 3H), 2.13–1.83 (m, 4H), 1.73–1.54 (m, 2H), 0.99–0.91 (m, 9H). ¹³C NMR (100 MHz, DMSO-*d*₆): δ 172.2, 171.8, 169.6, 169.2, 161.3, 152.0, 151.9, 149.5, 148.2, 139.9, 139.6, 131.6, 130.2, 129.4, 129.2, 128.6, 128.0, 122.6, 120.7, 108.4, 108.2, 108.2, 103.8, 101.0, 75.3, 75.3, 75.2, 69.4, 67.5, 67.3, 59.2, 57.1, 56.5, 56.2, 47.5, 47.4, 42.2, 38.4, 36.7, 36.4, 30.9, 30.8, 26.8, 26.7, 16.4, 16.4. LCMS (ESI⁺): calcd for C₄₅H₅₃N₉O₇S = 863.4, found, [M + H]⁺ = 864.4, *t*_R = 2.09 min. HRMS (ESI): *m/z* [M + H]⁺ Calcd for C₄₅H₅₃N₉O₇S, 864.3859; found, 864.3855.

N-(4-(4-((S)-1-((2S,4R)-4-Hydroxy-2-((S)-1-(4-(4-methylthiazol-5-yl)phenyl)ethyl)carbamoyl)pyrrolidin-1-yl)-3,3-dimethyl-1-oxobutan-2-yl)amino)-2-oxoethoxy)piperidin-1-yl)-2-methoxyphenyl)-6-(1H-pyrazol-5-yl)picolinamide (Degrader-3). 2-((1-(4-(6-(1H-Pyrazol-5-yl)picolinamido)-3-methoxyphenyl)piperidin-4-yl)oxy)acetic acid hydrochloride (13) (650 mg, 1.33 mmol), (2S,4R)-1-((S)-2-amino-3,3-dimethylbutanoyl)-4-hydroxy-N-((S)-1-(4-(4-methylthiazol-5-yl)phenyl)ethyl)pyrrolidine-2-carboxamide hydrochloride (14) (641 mg, 1.33 mmol), HOBt (269 mg, 1.99 mmol), DIPEA (516 mg, 3.99 mmol), and DMF (5 mL) were added to a 50 mL round-bottomed flask. Then, EDCI HCl (381 mg, 1.99 mmol) was added to the mixture. The reaction mixture was stirred at 40 °C for 2 h. The reaction mixture was purified by prep-HPLC (column: Phenomenex Synergi Max-RP 250*50 mm*10 μm, mobile phase A: water (0.225%FA), mobile phase B: acetonitrile, flow rate: 60 mL/min, and gradient condition: from 35% B to 65% B). The pure fractions were collected, and the solvent was evaporated under vacuum to give a residue, which was lyophilized to give the product as a yellow powder (218.5 mg, 18.7%). ¹H NMR (400 MHz, DMSO-*d*₆): δ 13.97–13.03 (m, 1H), 10.58 (br s, 1H), 8.98 (s, 1H), 8.48 (d, *J* = 7.6 Hz, 1H), 8.27–7.87 (m, 5H), 7.47–7.33 (m, 5H), 6.99 (br s, 1H), 6.74 (br s, 1H), 6.61–6.54 (m, 1H), 5.21–5.00 (m, 1H), 4.94–4.84 (m, 1H), 4.59–4.41 (m, 2H), 4.28 (br s, 1H), 4.10–3.90 (m, 5H), 3.63–3.49 (m, 5H), 3.00–2.88 (m, 2H), 2.45 (s, 3H), 2.11–1.95 (m, 3H), 1.80–1.57 (m, 3H), 1.50–1.34 (m, 3H), 0.94 (s, 9H). ¹³C NMR (100 MHz, DMSO-*d*₆): δ 170.9, 170.0, 169.5, 169.2, 168.5, 163.5, 161.2, 161.2, 151.9, 149.6, 148.2, 145.3, 145.0, 139.6, 131.6, 130.2, 130.1, 129.4, 129.3, 126.8, 122.5, 120.7, 107.8, 103.8, 103.8, 100.7, 75.5, 69.3, 67.4, 67.3, 59.2, 59.0, 57.1, 56.5, 56.1, 48.3, 47.0, 38.2, 36.7, 36.4, 31.0, 30.9, 26.8, 26.7, 23.0, 22.6, 16.5. LCMS (ESI⁺): calcd for C₄₆H₅₅N₉O₇S = 877.4, found, [M + H]⁺ = 878.4, *t*_R = 4.5 min. HRMS (ESI): *m/z* [M + H]⁺ Calcd for C₄₆H₅₅N₉O₇S, 878.4023; found, 878.4036.

N-(4-(4-((S)-1-((2S,4S)-4-Hydroxy-2-((S)-1-(4-(4-methylthiazol-5-yl)phenyl)ethyl)carbamoyl)pyrrolidin-1-yl)-3,3-di-

methyl-1-oxobutan-2-yl)amino)-2-oxoethoxy)piperidin-1-yl)-2-methoxyphenyl)-6-(1H-pyrazol-5-yl)picolinamide (Degrader-4). 2-((1-(4-(6-(1H-pyrazol-5-yl)picolinamido)-3-methoxyphenyl)piperidin-4-yl)oxy)acetic acid (**12**) (46 mg, 0.102 mmol), (2S,4S)-1-((S)-2-amino-3,3-dimethylbutanoyl)-4-hydroxy-N-((S)-1-(4-(4-methylthiazol-5-yl)phenyl)ethyl)pyrrolidine-2-carboxamide (**15**) (49.5 mg, 0.103 mmol), HOBt (20.7 mg, 0.153 mmol), DIPEA (39.6 mg, 0.306 mmol), and DMF (1 mL) were added to a 50 mL round-bottomed flask. Then, EDCI·HCl (29.4 mg, 0.153 mmol) was added to the mixture. The reaction mixture was stirred at 40 °C for 12 h. The mixture was poured into water (10 mL) and extracted by ethyl acetate (30 mL × 3). The organic layer was collected and dried over Na₂SO₄, filtered, and concentrated to give the residue, which was purified by prep-HPLC (column: DuraShell 150*25 mm*5 μm, mobile phase A: water (0.2% FA), mobile phase B: acetonitrile, flow rate: 25 mL/min, and gradient condition: from 28% B to 58%). The pure fractions were collected, and the solvent was evaporated under vacuum to give a residue, which was lyophilized to give the product as a yellow powder (20.9 mg, 23.4%). ¹H NMR (400 MHz, DMSO-*d*₆): δ 13.88 (br s, 0.2H), 13.22 (br s, 0.6H), 10.63–10.35 (m, 1H), 8.97 (s, 1H), 8.47–7.50 (m, 6H), 7.47–7.33 (m, 5H), 6.98 (br s, 1H), 6.73 (br s, 1H), 6.61–6.54 (m, 1H), 5.38–5.31 (m, 1H), 4.96–4.87 (m, 1H), 4.52 (d, *J* = 9.0 Hz, 1H), 4.44–4.31 (m, 1H), 4.26–4.17 (m, 1H), 4.09–3.74 (m, 6H), 3.60–3.43 (m, 4H), 3.00–2.87 (m, 2H), 2.46–2.43 (m, 3H), 2.39–2.31 (m, 1H), 2.05–1.91 (m, 2H), 1.72–1.54 (m, 3H), 1.38 (m, 3H), 1.03–0.88 (m, 9H). ¹³C NMR (100 MHz, DMSO-*d*₆): δ 171.3, 170.1, 169.7, 169.4, 161.2, 151.9, 149.6, 148.2, 144.8, 139.6, 131.6, 130.3, 129.3, 126.8, 122.5, 120.7, 107.8, 100.7, 75.5, 69.4, 67.8, 67.2, 58.9, 56.5, 56.2, 56.0, 48.3, 47.0, 37.3, 36.6, 35.9, 31.0, 30.9, 26.9, 26.7, 22.8, 22.4, 16.4. LCMS (ESI⁺): calcd for C₄₆H₅₅N₉O₇S = 877.4, found, [M + H]⁺ = 878.4, *t*_R = 4.22 min. HRMS (ESI): *m/z* [M + H]⁺ calcd for C₄₆H₅₅N₉O₇S, 878.4023; found, 878.4009.

■ ASSOCIATED CONTENT

Supporting Information

The Supporting Information is available free of charge at <https://pubs.acs.org/doi/10.1021/acs.jmedchem.1c00103>.

Western blot validation of proteomics studies of **Degrader-3**; global proteomic data of **Degrader-3** in HBL-1 cells; anti-proliferative potency of **JH-I-25** in HBL-1 cells; Western blot of IRAK1 and IRAK4 protein degradation in HEK293T cells; kinase activity assay; VHL FP assay; immunoblotting protocol; cell culture and cell viability assay; global proteomics assay protocol; ¹H NMR and ¹³C NMR spectra for conjugates **Degrader-1**, **Degrader-2**, **Degrader-3**, and **Degrader-4**; and KinomeScan raw data of **JH-I-25**, **Degrader-3**, and **Degrader-4** (PDF)

Proteomics raw data of **Degrader-3** in Toledo (CSV)

Proteomics raw data of **Degrader-3** in HBL-1 (CSV)

■ AUTHOR INFORMATION

Corresponding Authors

Jennifer D. Venable – Discovery Sciences, Janssen Research & Development, San Diego, California 92121, United States; Email: jvenable@its.jnj.com

Xuedong Dai – Discovery Sciences, Janssen (China) Research & Development, Shanghai 201210, P.R. China; Discovery Chemistry, Janssen Research & Development, Shanghai 201210, China; orcid.org/0000-0003-4358-0319; Email: xdai18@its.jnj.com

Authors

Liqiang Fu – Discovery Chemistry, Janssen Research & Development, Shanghai 201210, China

Jing Zhang – Department of Biology, Janssen Research & Development, Shanghai 201210, China

Bin Shen – Department of Biology, Janssen Research & Development, Shanghai 201210, China

Linglong Kong – Discovery Chemistry, Janssen Research & Development, Shanghai 201210, China

Yingtao Liu – Discovery Chemistry, Janssen Research & Development, Shanghai 201210, China

Wangyang Tu – Discovery Chemistry, Janssen Research & Development, Shanghai 201210, China

Wenqian Wang – Department of Biology, Janssen Research & Development, Shanghai 201210, China

Xin Cai – Department of Biomarker, Janssen Research & Development, Shanghai 201210, China

Xiaotao Wang – Department of Biomarker, Janssen Research & Development, Shanghai 201210, China

Na Cheng – Department of Biology, Janssen Research & Development, Shanghai 201210, China

Mingxuan Xia – Department of Biology, Janssen Research & Development, Shanghai 201210, China

Tianyuan Zhou – Department of Biology, Janssen Research & Development, Shanghai 201210, China

Qian Liu – Discovery Chemistry, Janssen Research & Development, Shanghai 201210, China

Yanping Xu – Discovery Chemistry, Janssen Research & Development, Shanghai 201210, China

Jennifer Yang – Department of Biology, Janssen Research & Development, Shanghai 201210, China

Paul Gavine – Department of Biology, Janssen Research & Development, Shanghai 201210, China

Ulrike Philipp – Janssen Pharmaceutical Research & Development, Beerse 2340, Belgium

Ricardo Attar – Janssen Pharmaceutical Research & Development, Spring House, Pennsylvania 19477, United States

James P. Edwards – Discovery Sciences, Janssen Research & Development, San Diego, California 92121, United States

Complete contact information is available at:

<https://pubs.acs.org/doi/10.1021/acs.jmedchem.1c00103>

Author Contributions

△L.F. and J.Z. contributed equally. L.F. wrote the original draft, J.Z., L.K., X.W., T.Z., P.G., J.P.E., J.D.V., and X.D. revised the draft, and all authors reviewed and edited the manuscript. All authors have given approval to the final version of the manuscript.

Notes

The authors declare no competing financial interest.

■ ACKNOWLEDGMENTS

The authors would like to thank the members of the Discovery Science and Oncology Translational Research team at Janssen including Charu Chaudhry and Haopeng Rui for insightful discussion and Yan Wang for help with graphical abstract design.

■ ABBREVIATIONS

ABC, activated B-cell-like; CRBN, cereblon; DIPEA, *N*, *N*-diisopropylethylamine; DLBCL, diffuse large B-cell lymphoma; DMF, dimethylformamide; EDCI, 1-ethyl-3-(3-dimethylaminopropyl)carbodiimide; EtOAc, ethyl acetate; GAK, cyclin G-associated kinase; GCB, center B-cell-like;

HATU, 1-*bis*(dimethylamino)methylene]-1*H*-1,2,3- triazolo-[4,5-*b*]pyridinium 3-oxide hexafluorophosphate; NHL, non-Hodgkin lymphoma; IL-1R, interleukin-1 receptor; IRAK1, interleukin-1 receptor-associated kinase 1; MAPK, mitogen-activated protein kinase; MyD88, myeloid differentiation primary response 88; NF- κ B, I κ B kinase (IKK)-nuclear factor- κ B; NMRAL1, NmrA-like family domain-containing protein 1; PROTACs, proteolysis-targeting chimeras; TEA, triethanolamine; TLRs, toll-like receptors; TRAF6, TNF receptor-associated factor 6; VHL, von Hippel–Lindau.

REFERENCES

- (1) De Nardo, D.; Balka, K. R.; Cardona Gloria, Y.; Rao, V. R.; Latz, E.; Masters, S. L. Interleukin-1 receptor-associated kinase 4 (IRAK4) plays a dual role in myddosome formation and Toll-like receptor signaling. *J. Biol. Chem.* **2018**, *293*, 15195–15207.
- (2) Lin, S.-C.; Lo, Y.-C.; Wu, H. Helical assembly in the MyD88-IRAK4-IRAK2 complex in TLR/IL-1R signalling. *Nature* **2010**, *465*, 885–890.
- (3) Roschewski, M.; Staudt, L. M.; Wilson, W. H. Diffuse large B-cell lymphoma-treatment approaches in the molecular era. *Nat. Rev. Clin. Oncol.* **2014**, *11*, 12–23.
- (4) Ngo, V. N.; Young, R. M.; Schmitz, R.; Jhavar, S.; Xiao, W.; Lim, K.-H.; Kohlhammer, H.; Xu, W.; Yang, Y.; Zhao, H.; Shaffer, A. L.; Romesser, P.; Wright, G.; Powell, J.; Rosenwald, A.; Muller-Hermelink, H. K.; Ott, G.; Gascoyne, R. D.; Connors, J. M.; Rimsza, L. M.; Campo, E.; Jaffe, E. S.; Delabie, J.; Smeland, E. B.; Fisher, R. I.; Braziel, R. M.; Tubbs, R. R.; Cook, J. R.; Weisenburger, D. D.; Chan, W. C.; Staudt, L. M. Oncogenically active MYD88 mutations in human lymphoma. *Nature* **2011**, *470*, 115–119.
- (5) Zhang, J.; Fu, L.; Shen, B.; Liu, Y.; Wang, W.; Cai, X.; Kong, L.; Yan, Y.; Meng, R.; Zhang, Z.; Chen, Y.-N. P.; Liu, Q.; Wan, Z.-K.; Zhou, T.; Wang, X.; Gavine, P.; Del Rosario, A.; Ahn, K.; Philippart, U.; Attar, R.; Yang, J.; Xu, Y.; Edwards, J. P.; Dai, X. Assessing IRAK4 functions in ABC DLBCL by IRAK4 kinase inhibition and protein degradation. *Cell Chem. Biol.* **2020**, *27*, 1500–1509.
- (6) Phelan, J. D.; Young, R. M.; Webster, D. E.; Roulland, S.; Wright, G. W.; Kasbekar, M.; Shaffer, A. L.; Ceribelli, M.; Wang, J. Q.; Schmitz, R.; Nakagawa, M.; Bachy, E.; Huang, D. W.; Ji, Y.; Chen, L.; Yang, Y.; Zhao, H.; Yu, X.; Xu, W.; Palisoc, M. M.; Valadez, R. R.; Davies-Hill, T.; Wilson, W. H.; Chan, W. C.; Jaffe, E. S.; Gascoyne, R. D.; Campo, E.; Rosenwald, A.; Ott, G.; Delabie, J.; Rimsza, L. M.; Rodriguez, F. J.; Estephan, F.; Holdhoff, M.; Kruhlak, M. J.; Hewitt, S. M.; Thomas, C. J.; Pittaluga, S.; Oellerich, T.; Staudt, L. M. A multiprotein supercomplex controlling oncogenic signalling in lymphoma. *Nature* **2018**, *560*, 387–391.
- (7) Reddy, A.; Zhang, J.; Davis, N. S.; Moffitt, A. B.; Love, C. L.; Waldrop, A.; Leppa, S.; Pasanen, A.; Meriranta, L.; Karjalainen-Lindsberg, M.-L.; Nørgaard, P.; Pedersen, M.; Gang, A. O.; Høgdall, E.; Heavican, T. B.; Lone, W.; Iqbal, J.; Qin, Q.; Li, G.; Kim, S. Y.; Healy, J.; Richards, K. L.; Fedoriw, Y.; Bernal-Mizrachi, L.; Koff, J. L.; Staton, A. D.; Flowers, C. R.; Paltiel, O.; Goldschmidt, N.; Calaminici, M.; Clear, A.; Gribben, J.; Nguyen, E.; Czader, M. B.; Ondrejka, S. L.; Collie, A.; Hsi, E. D.; Tse, E.; Au-Yeung, R. K. H.; Kwong, Y.-L.; Srivastava, G.; Choi, W. W. L.; Evens, A. M.; Pilichowska, M.; Sengar, M.; Reddy, N.; Li, S.; Chadburn, A.; Gordon, L. I.; Jaffe, E. S.; Levy, S.; Rempel, R.; Tzeng, T.; Happ, L. E.; Dave, T.; Rajagopalan, D.; Datta, J.; Dunson, D. B.; Dave, S. S. Genetic and functional drivers of diffuse large B cell lymphoma. *Cell* **2017**, *171*, 481–494.
- (8) Hatcher, J. M.; Yang, G.; Wang, L.; Ficarro, S. B.; Buhrlage, S.; Wu, H.; Marto, J. A.; Treon, S. P.; Gray, N. S. Discovery of a selective, covalent IRAK1 inhibitor with antiproliferative activity in MYD88 mutated B-cell lymphoma. *ACS Med. Chem. Lett.* **2020**, *11*, 2238–2243.
- (9) Burslem, G. M.; Crews, C. M. Small-molecule modulation of protein homeostasis. *Chem. Rev.* **2017**, *117*, 11269–11301.
- (10) Churcher, I. Protac-induced protein degradation in drug discovery: breaking the rules or just making new ones? *J. Med. Chem.* **2018**, *61*, 444–452.
- (11) Pettersson, M.; Crews, C. M. PROTeolysis TArgeting Chimeras (PROTACs)—past, present and future. *Drug Discov. Today Technol.* **2019**, *31*, 15–27.
- (12) Verma, R.; Mohl, D.; Deshaies, R. J. Harnessing the power of proteolysis for targeted protein inactivation. *Mol. Cell* **2020**, *77*, 446–460.
- (13) Buckley, G. M.; Gowers, L.; Higuero, A. P.; Jenkins, K.; Mack, S. R.; Morgan, T.; Parry, D. M.; Pitt, W. R.; Rausch, O.; Richard, M. D.; Sabin, V.; Fraser, J. L. IRAK-4 inhibitors. Part 1: a series of amides. *Bioorg. Med. Chem. Lett.* **2008**, *18*, 3211–3214.
- (14) Wang, L.; Qiao, Q.; Ferrao, R.; Shen, C.; Hatcher, J. M.; Buhrlage, S. J.; Gray, N. S.; Wu, H. Crystal structure of human IRAK1. *Proc. Natl. Acad. Sci. U. S. A.* **2017**, *114*, 13507–13512.
- (15) Hansen, J. D.; Correa, M.; Nagy, M. A.; Alexander, M.; Plantevin, V.; Grant, V.; Whitefield, B.; Huang, D.; Kercher, T.; Harris, R.; Narla, R. K.; Leisten, J.; Tang, Y.; Moghaddam, M.; Ebinger, K.; Piccotti, J.; Havens, C. G.; Cathers, B.; Carmichael, J.; Daniel, T.; Vessey, R.; Hamann, L. G.; Leftheris, K.; Mendy, D.; Baculi, F.; LeBrun, L. A.; Khambatta, G.; Lopez-Girona, A. Discovery of CRBN E3 ligase modulator CC-92480 for the treatment of relapsed and refractory multiple myeloma. *J. Med. Chem.* **2020**, *63*, 6648–6676.
- (16) Matyskiela, M. E.; Lu, G.; Ito, T.; Pagarigan, B.; Lu, C.-C.; Miller, K.; Fang, W.; Wang, N.-Y.; Nguyen, D.; Houston, J.; Carmel, G.; Tran, T.; Riley, M.; Nosaka, L. A.; Lander, G. C.; Gaidarova, S.; Xu, S.; Ruchelman, A. L.; Handa, H.; Carmichael, J.; Daniel, T. O.; Cathers, B. E.; Lopez-Girona, A.; Chamberlain, P. P. A novel cereblon modulator recruits GSPT1 to the CRL4(CRBN) ubiquitin ligase. *Nature* **2016**, *535*, 252–257.
- (17) Matyskiela, M. E.; Couto, S.; Zheng, X.; Lu, G.; Hui, J.; Stamp, K.; Drew, C.; Ren, Y.; Wang, M.; Carpenter, A.; Lee, C.-W.; Clayton, T.; Fang, W.; Lu, C.-C.; Riley, M.; Abdubek, P.; Blease, K.; Hartke, J.; Kumar, G.; Vessey, R.; Rolfe, M.; Hamann, L. G.; Chamberlain, P. P. SALL4 mediates teratogenicity as a thalidomide-dependent cereblon substrate. *Nat. Chem. Biol.* **2018**, *14*, 981–987.
- (18) Asatsuma-Okumura, T.; Ando, H.; De Simone, M.; Yamamoto, J.; Sato, T.; Shimizu, N.; Asakawa, K.; Yamaguchi, Y.; Ito, T.; Guerrini, L.; Handa, H. p63 is a cereblon substrate involved in thalidomide teratogenicity. *Nat. Chem. Biol.* **2019**, *15*, 1077–1084.
- (19) Hagner, P. R.; Man, H.-W.; Fontanillo, C.; Wang, M.; Couto, S.; Breider, M.; Bjorklund, C.; Havens, C. G.; Lu, G.; Rychak, E.; Raymon, H.; Narla, R. K.; Barnes, L.; Khambatta, G.; Chiu, H.; Kosek, J.; Kang, J.; Amantangelo, M. D.; Waldman, M.; Lopez-Girona, A.; Cai, T.; Pourdehnad, M.; Trotter, M.; Daniel, T. O.; Schafer, P. H.; Klippel, A.; Thakurta, A.; Chopra, R.; Gandhi, A. K. CC-122, a pleiotropic pathway modifier, mimics an interferon response and has antitumor activity in DLBCL. *Blood* **2015**, *126*, 779–789.
- (20) Galdeano, C.; Gadd, M. S.; Soares, P.; Scaffidi, S.; Van Molle, I.; Birced, I.; Hewitt, S.; Dias, D. M.; Ciulli, A. Structure-guided design and optimization of small molecules targeting the protein-protein interaction between the von Hippel-Lindau (VHL) E3 ubiquitin ligase and the hypoxia inducible factor (HIF) alpha subunit with in vitro nanomolar affinities. *J. Med. Chem.* **2014**, *57*, 8657–8663.
- (21) Soares, P.; Gadd, M. S.; Frost, J.; Galdeano, C.; Ellis, L.; Epemolu, O.; Rocha, S.; Read, K. D.; Ciulli, A. Group-based optimization of potent and cell-active inhibitors of the von Hippel-Lindau (VHL) E3 ubiquitin ligase: structure-activity relationships leading to the chemical probe (2*S*,4*R*)-1-((*S*)-2-(1-cyanocyclopropyl)carboxamido)-3,3-dimethylbutanoyl)-4-hydroxy-N-(4-(4-methylthiazol-5-yl)benzyl)pyrrolidine-2-carboxamide (VH298). *J. Med. Chem.* **2018**, *61*, 599–618.
- (22) Hu, J.; Hu, B.; Wang, M.; Xu, F.; Miao, B.; Yang, C.-Y.; Wang, M.; Liu, Z.; Hayes, D. F.; Chinnaswamy, K.; Delproposto, J.; Stuckey, J.; Wang, S. Discovery of ERD-308 as a highly potent proteolysis

targeting chimera (PROTAC) degrader of estrogen receptor (ER). *J. Med. Chem.* **2019**, *62*, 1420–1442.

(23) Gütschow, M.; Steinebach, C.; Voell, S. A.; Vu, L. P.; Bricelj, A.; Sosič, I.; Schnakenburg, G. A facile synthesis of ligands for the von Hippel–Lindau E3 ligase. *Synthesis* **2020**, *52*, 2521–2527.

(24) Bondeson, D. P.; Smith, B. E.; Burslem, G. M.; Buhimschi, A. D.; Hines, J.; Jaime-Figueroa, S.; Wang, J.; Hamman, B. D.; Ishchenko, A.; Crews, C. M. Lessons in PROTAC design from selective degradation with a promiscuous warhead. *Cell Chem. Biol.* **2018**, *25*, 78–87.

(25) Kostic, M.; Jones, L. H. Critical assessment of targeted protein degradation as a research tool and pharmacological modality. *Trends Pharmacol. Sci.* **2020**, *41*, 305–317.

(26) Lenz, G. Insights into the molecular pathogenesis of activated B-cell-like diffuse large B-cell lymphoma and its therapeutic implications. *Cancers (Basel)* **2015**, *7*, 811–822.

(27) Ferreiro, D. U.; Komives, E. A. Molecular mechanisms of system control of NF- κ B signaling by IkappaB α . *Biochemistry* **2010**, *49*, 1560–1567.

(28) Buckley, D. L.; Raina, K.; Darricarrere, N.; Hines, J.; Gustafson, J. L.; Smith, I. E.; Miah, A. H.; Harling, J. D.; Crews, C. M. HaloPROTACS: use of small molecule PROTACs to induce degradation of HaloTag fusion proteins. *ACS Chem. Biol.* **2015**, *10*, 1831–1837.